IL NUOVO CIMENTO **47 C** (2024) 292
DOI 10.1393/ncc/i2024-24292-7

COMMUNICATIONS: SIF Congress 2023

Tight-binding simulation of ultrafast pulse-assisted field emission from a metallic tip

L. J. D'ONOFRIO(1)(2)(3)(*), A. AVELLA(1)(3)(4) and M. ECKSTEIN(2)(5)

(1) *Dipartimento di Fisica "E.R. Caianiello", Università degli Studi di Salerno I-84084 Fisciano (SA), Italy*
(2) *Department of Physics, University of Erlangen-Nürnberg - 91058 Erlangen, Germany*
(3) *CNR-SPIN, UoS di Salerno - I-84084 Fisciano (SA), Italy*
(4) *Unità CNISM di Salerno, Università degli Studi di Salerno - I-84084 Fisciano (SA), Italy*
(5) *Institute of Theoretical Physics, University of Hamburg - 22607 Hamburg, Germany*

received 29 January 2024

Summary. — Field emission is a powerful technique to gain insight into the electronic properties of materials. A strong and ultrashort laser pulse can periodically modify the potential barrier for electron tunnelling, giving rise to photon sidebands in the far-field electron energy distribution. The aim of this work is to present a novel tight-binding approach that simulates the laser-assisted field emission from a metallic tip taking account also of the electronic features of the emitter. The out-of-equilibrium electron dynamics of this inhomogeneous system is described using the Green's function formalism.

1. – Introduction

The field emission technique has always played a central role in the world of condensed matter physics [1]. In particular, nowadays, the emergence of modern laser technologies [2] has determined a growing interest in the study of ultrafast laser-stimulated field emission processes, especially for the possibility of generating electronic pulses with a simultaneous high spatial and time resolution [3-5]. Reaching this aim is subject to the necessity of identifying the class of materials that could ensure an efficient electronic emission on a very short timescale.

Here, we present a novel theoretical approach able to reconstruct the energy distribution that laser-driven field-emitted electrons have in a region of space far from the emitter-vacuum interface, including the properties of the emitter through tight-binding methods and non-equilibrium techniques.

2. – Model

Let us start from a metallic tip in equilibrium at a temperature T for $t \to -\infty$. Due to a high work-function ϕ, electrons are confined within the metal until, at $t = 0$, a voltage difference $|V_{pot}|$ is applied between the end of the tip and an electrode, bending

(*) Corresponding author. E-mail: lucianojacopo.donofrio@spin.cnr.it

the step potential barrier and letting electrons tunnel into the vacuum. They can so reach the *far-field region* —a region of space sufficiently far from the solid-vacuum interface— where their energy distribution is measured. Then, at $t = t_0$, an ultrafast laser pulse is switched on in proximity to the metal-vacuum interface, modifying the barrier profile and affecting the electronic emission process from the tip. The tight-binding Hamiltonian that models this situation can be written as follows (the spin index is discarded in this work):

$$\hat{\mathcal{H}}(t) = \sum_{i=1}^{T-1}(-t_i(t)\hat{c}_i^\dagger\hat{c}_{i+1} + \text{h.c.}) + \sum_{i=1}^{T}(\epsilon_i(t) - \mu)\hat{n}_i. \tag{1}$$

Here $T = N+M$ is the total number of sites of this two-chain system: the first chain (with N sites) models a very sharp and thin metallic tip; instead, the second one (with M sites) discretizes the vacuum along the direction of propagation normal to the tip surface [6,7]. $\hat{c}_i$ ($\hat{c}_i^\dagger$) annihilates (creates) an electron on the i-th site of such an inhomogeneous (matter+vacuum) system and, thus, t_i is the *nearest-neighbor hopping integral* between the i-th and the $(i+1)$-th site. By considering a homogeneous and isotropic tip, we can put $t_i = t_m$ for $i < N$, where $4t_m$ corresponds to the width of the single-electron band within the uncorrelated emitting metal (electron-electron interactions are considered negligible). Similarly, by putting $t_i = t_v$ for $i > N$, the energy of an electron with momentum k in the far-field region, *i.e.*, $\varepsilon(k) = \phi - e|V_{pot}| + (\hbar k)^2/2m$, can be properly approximated by the tight-binding cosine dispersion $\varepsilon_{ff}(k) = \phi - e|V_{pot}| + 2t_v(1 - \cos(kb))$, with $4t_v$ as its band-width and $b = \hbar/\sqrt{2mt_v}$ as the *vacuum lattice constant*. In addition, the term $(-t_N(t)\hat{c}_N^\dagger\hat{c}_{N+1} + \text{h.c.})$ lets electrons jump between the last matter site and the first vacuum one. Indeed, after the switching-on of the voltage difference $|V_{pot}|$, electrons can be emitted into the vacuum from the tip edge and, therefore, this process must be included in the Hamiltonian. Furthermore, by choosing

$$t_N(t) = \begin{cases} t_c \sin^4(\pi t/2\tau_{ad}), & 0 \le t \le \tau_{ad}, \\ t_c, & t > \tau_{ad} \end{cases}$$

with $\tau_{ad} \ll t_0$, we assume an adiabatic preparation of the state reached by the system after the application of $|V_{pot}|$. In the second term of $\hat{\mathcal{H}}$, where μ is the chemical potential and $\hat{n}$ is the number operator, the mean on-site electronic energy ϵ_i is put equal to ϵ_m inside the metal ($i \le N$), while, for $i > N$, it contains the time- and space-dependent profile of the barrier V faced by the electrons in the vacuum: $\epsilon_i(t) = 2t_v + eV_i(t)$. The Hamiltonian operator can be so recast in a more compact form: $\hat{\mathcal{H}}(t) = \sum_{i,j=1}^{T}\hat{c}_i^\dagger h_{i,j}(t)\hat{c}_j$, with $\{H(t)\}_{i,j} = h_{i,j}(t) = \delta_{i,j}\epsilon_i(t) - t_{i-1}^*(t)\delta_{i,j+1} - t_i(t)\delta_{i+1,j}$.

To get the energy distribution of electrons in the far-field region, we exploit the Green's functions formalism considering the lesser components $\{G^<(t,t')\}_{i,j} = g_{i,j}^<(t,t')$ in the Keldysh framework [8,9]. Dealing with an independent-particle model, we can express, at a given time t, the fermionic operators in the Heisenberg picture in terms of the elements of the complete set $\{\hat{c}_i, \hat{c}_i^\dagger\}_{i=1,\dots,T}$ as $\hat{c}_{i,H}(t) = \sum_j \hat{u}_{i,j}(t, t' \to -\infty)\hat{c}_j$, where $\hat{c}_i^{(\dagger)} = \hat{c}_{i,H}^{(\dagger)}(t \to -\infty)$ and $\{\hat{U}(t,t')\}_{i,j} = \hat{u}_{i,j}(t,t')$ acts like a single-particle time-evolution operator such that $i\hbar\partial_t\hat{U}(t,t') = H(t)\cdot\hat{U}(t,t')$. Then, once the far-field submatrix of $G^<$ is computed solving the equation of motion for $\hat{U}$, its elements can be combined in a Fourier series to get the lesser Green's function in k-space, *i.e.*, $g_k^< = g_k^<(t,t')$. The

mean far-field time-dependent electron energy distribution can be, thus, constructed: $\langle n \rangle (\varepsilon, t) = \sum_k \langle n_k \rangle (t) = -i \sum_k g_k^<(t,t)$, where the sum is over all the k-points such that $\varepsilon = \varepsilon_{ff}(k)$. That quantity depends clearly on the electronic bunches that, after being emitted, propagate towards the detector through time. If we wait enough such that all the extracted electrons can reach the far-field region ($t \to \infty$), such a distribution will not depend on time anymore. Thus, from here on, we will focus on the *latest-time* far-field energy distribution.

3. – Results

We choose a space decaying barrier profile $V = V(x,t)$, for $x \geq 0$ and $t \geq 0$. Moreover, the pulse acts only close to the tip-vacuum interface [6, 7], where it determines oscillations in time of the *barrier width* B_w [10]. This setting is modelled with the voltage profile $V_i(t) = \frac{\phi}{e} - |V_{pot}|[1 - \exp(\frac{-(i-N-1)bK}{B_w(t)})]$, for $i \geq N+1$, $K = \ln(\frac{e|V_{pot}|}{e|V_{pot}|-\phi})$, with time-dependent barrier width $B_w(t) = B_w^0(1+F(t))$. $F(t) = F\cos(\frac{2\pi}{T_{\rm per}}(t-t_0)+\varphi) \times \exp(-\frac{(t-t_0)^2}{2\tau_P^2})$ identifies the percentage deviation in time of the barrier width with respect to B_w^0, where $F \geq 0$ depends on the pulse intensity, while T_{per}, φ, and τ_P are the pulse period, phase, and width, respectively. The results of this work are obtained considering $N = 500$ matter sites and $M = 2600$ vacuum ones. A study is, thus, performed changing T_{per} and t_m. So, we fix $\epsilon_m = \mu = 0\,\text{eV}$, $\phi = 5\,\text{eV}$, $|V_{pot}| = 10\,\text{V}$, $t_v = 10\,\text{eV}$, and $B_w^0 = 1\,\text{nm}$. Furthermore, we focus on the case of an ultrafast pulse sufficiently intense such that $F = 0.9$; in addition, $t_0 = 30\,\text{fs}$, $\tau_P = 4\,\text{fs}$, and $\varphi = 0$. Finally, $\tau_{ad} = 1\,\text{fs}$ and $t_c = 1\,\text{eV}$. Thus, the far-field ($i \geq 900$) energy distribution at $t = t_{fin} \gg t_0$ is inferred through the aforementioned procedure.

The latest-time far-field energy distributions for $t_m = 1\,\text{eV}$ and for $T_{per} = 0.5$, 1, 2 fs are plotted in fig. 1(a). As expected [6], *photon sidebands* emerge clearly in all the considered cases. This aspect can be initially appreciated by noticing that, when T_{per}

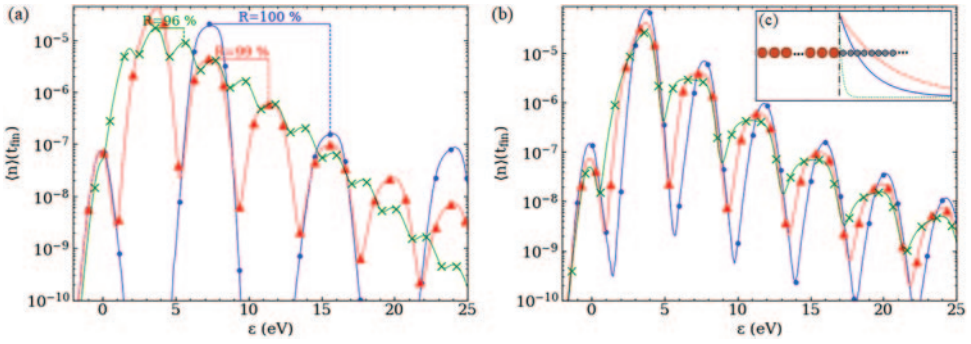

Fig. 1. – (a) Latest-time far-field electronic energy distribution for $T_{per} = 0.5\,\text{fs}$ (blue points), $T_{per} = 1\,\text{fs}$ (red triangles), and $T_{per} = 2\,\text{fs}$ (green crosses), having fixed $t_m = 1\,\text{eV}$. The energy distance between two consecutive peaks is plotted with the corresponding ratio R in each case. (b) Same quantity plotted in (a) for $T_{per} = 1\,\text{fs}$, but with $t_m = 0.5\,\text{eV}$ (blue points), $t_m = 1\,\text{eV}$ (red triangles), and $t_m = 1.5\,\text{eV}$ (green ×'s). In the insert (c), the metallic (brown sites) and the vacuum (gray sites) chains are schematically reported along with a sketch of the vacuum barrier profile (in arbitrary units) faced by the electrons at $t = 0$ (solid blue line), $t = t_0$ (dashed red line), and $t = t_0 + T_{per}/2$ (dotted green line).

doubles, the distance between two consecutive peaks results to be halved, as the photon energy does. In addition, by performing a multigaussian fit of the results in each case, the ratio R of the energy distance ΔE between two consecutive peaks and the corresponding photon energy $\varepsilon_{ph} = h/T_{per}$ is approximately 1 in all three illustrative cases. Therefore, the peaks in the energy distribution can be interpreted as a consequence of different electronic multiphoton excitations from the solid energy states. In fig. 1(b), it is shown $\langle n \rangle(\varepsilon, t_{fin})$ for $T_{per} = 1\,\mathrm{fs}$ and $t_m = 0.5,\ 1,\ 1.5\,\mathrm{eV}$. In agreement with our predictions, the positions of the peaks are not substantially affected by the value of t_m. On the other hand, it carries weight in determining the height and width of the photon sidebands. That feature can be understood considering that, by increasing t_m, the solid density of states results to be broadened in energy and lowered around the Fermi level. Such a modification is so reflected in the far-field energy distribution with wider sidebands and lowered peaks, underlying that the solid electronic properties are somehow transferred in the single-particle energy distribution even if detected very far from the solid itself.

4. – Conclusions

In this work, we have presented a minimal theoretical setup able to simulate the laser-stimulated field emission of electrons from a metallic tip. The final aim has been to compute the latest-time far-field electronic energy distribution varying the pulse frequency and the equilibrium density of states of the emitter. From the results, we have understood that our model is capable of predicting the presence of photon sidebands in the far-field distribution due to multiphoton excitations of electrons from the tip. In addition, thanks to the model, it has been possible to appreciate how the far-field energy distribution is affected by the metallic density of states, pioneering possible interpretations of experimental results in terms of the emitter features. Finally, through our framework, further studies about the activation of multiphoton excitations could be carried out, especially for their role in the high-harmonics generation in solids [11]. Particularly, some efforts could be devoted to understanding how the appearance of such processes is related to the laser pulse properties and whether, in this case, signatures of resulting non-linear effects become manifest in the matter density of states.

* * *

LJD and AA acknowledge support by MIUR under Project No. PRIN 2017RKWTMY. LJD acknowledges support by EU under the Erasmus Plus Traineeship program.

REFERENCES

[1] Bonard J.-M. *et al.*, *Appl. Phys. A*, **69** (1999) 245.
[2] Krausz F. and Ivanov M., *Rev. Mod. Phys.*, **81** (2009) 163.
[3] Hommelhoff P. *et al.*, *Phys. Rev. Lett.*, **96** (2006) 077401.
[4] Ropers C. *et al.*, *Phys. Rev. Lett.*, **98** (2007) 043907.
[5] Hommelhoff P. *et al.*, *Phys. Rev. Lett.*, **97** (2006) 247402.
[6] Krüger M. *et al.*, *New J. Phys.*, **14** (2012) 085019.
[7] Schenk M. *et al.*, *Phys. Rev. Lett.*, **105** (2010) 257601.
[8] Aoki H. *et al.*, *Rev. Mod. Phys.*, **86** (2014) 779.
[9] van Leeuwen R. A. *et al.*, *Lect. Notes Phys.*, **706** (2006) 33.
[10] Zhang P. and Lau Y. Y., *Sci. Rep.*, **6** (2016) 19894.
[11] Ghimire S. and Reis D. A., *Nat. Phys.*, **15** (2019) 10.